G. Panzarasa, A. Osypova, G. Consolati, S. Pandini
Microsegregating Blends of Ethyl Cellulose and Poly(vinyl Pyrrolidone): a Combined Thermo-Mechanical and Positron Annihilation Spectroscopy Study
Cellulose, Vol. 26, N. 3, 2019, p. 1619-1630
doi:10.1007/s10570-018-2220-6

Microsegregating Blends of Ethyl Cellulose and Poly(vinyl pyrrolidone): a Combined Thermo-Mechanical and Positron Annihilation Spectroscopy Study

Guido Panzarasa[1], Alina Osypova[2], Giovanni Consolati[3,4], Stefano Pandini[5]*

1. Laboratory for Soft and Living Materials, Department of Materials, ETH Zürich, Vladimir-Prelog-Weg 5, 8093 Zürich, Switzerland.
2. Innovative Sensor Technology, IST AG Stegrütistrasse 14, 9462 Ebnat-Kappel, Switzerland.
3. Department of Aerospace Science and Technology, Politecnico di Milano, via La Masa 34, 20156 Milano, Italy.
4. INFN, sezione di Milano, via Celoria 16, 20133 Milano, Italy.
5. Department of Mechanical and Industrial Engineering, University of Brescia, Via Branze 38, Brescia 25123, Italy

*Corresponding author. E-mail: gp4779@gmail.com ; guidop@ethz.ch. Tel.: +41 44 633 92 48.

Guido Panzarasa ORCID: 0000-0003-1044-0491

Alina Osypova ORCID: 0000-0001-6953-5124

Giovanni Consolati ORCID: 0000-0003-3614-245X

Stefano Pandini ORCID: 0000-0003-2390-8495

Abstract

Polymer blends are a versatile playground for studying phase separation and its effect on the development of morphology and mechanical properties of the resulting materials. Blends obtained from two immiscible polymers, ethyl cellulose (EC) and poly(vinyl pyrrolidone) (PVP), are especially relevant for their practical applications as coatings for pharmaceutical preparations and controlled drug release. Here, films of EC-PVP blends are studied by means of thermal analysis, dynamic-mechanical analysis as well as positron annihilation lifetime spectroscopy. The morphology of the microstructures generated by phase separation is investigated by means of scanning electron microscopy. The effect of both components' ratio and of molecular mass of PVP on the final properties of the blends is determined in a systematical way. The results obtained are not only of theoretical interest but will prove useful for the optimization of industrial formulations based on these polymers.

Graphical abstract

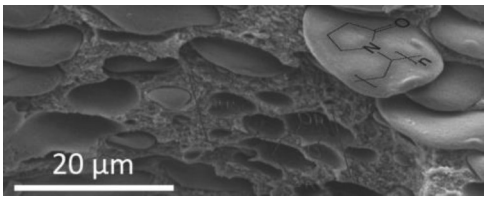

Keywords

Ethyl cellulose; poly(vinyl pyrrolidone); polymer blends; phase segregation; thermo-mechanical analysis; positron annihilation lifetime spectroscopy.

Introduction

Polymer blends are mechanical mixtures of two or more different polymers. They allow to obtain materials with improved properties without the need to chemically modify the structure of the individual polymers. For this reason, polymer blends are an important subject of investigation from both the theoretical and applicative viewpoint.

The miscibility of polymers is governed mainly by entropic factors and many polymer blends are thermodynamically immiscible because of a small combinatorial entropy value (*e.g.* due to excessively high molecular masses), as can be derived from a Flory-Huggins description of the system's thermodynamics (Robeson 2007). Immiscibility can result, under appropriate conditions, in phase separation. Eventually, the properties of the blend will be determined by miscibility and phase behavior. The mechanisms for phase separation of binary polymer blends, both in bulk and in thin films, have been the subject of extensive studies over decades and are nowadays well understood. Depending on the nature of the interactions between the individual components, polymer blends may be miscible (single-phase), partially miscible or immiscible (phase-separated). Obtaining a one-phase system with polymer blends usually requires to ensure that favourable, specific intermolecular interactions, such as hydrogen bonding, exist between the components of the blend (Barlow and Paul 1981; Utracki 1991; Pernot et al. 2002; Imre and Pukánszky 2013).

Thermal analysis, and especially the measurement of glass transition temperature T_g, is a common approach to study the behavior of polymer blends (Brostow et al. 2008). Miscible blends will exhibit a single T_g at an intermediate value between the T_gs of the individual components. In immiscible blends, the T_gs of the individual components will remain unchanged. Partial miscibility occurs when the solubility limit of one of the polymers in a miscible blend is exceeded, resulting in phase separation and in an additional T_g corresponding to the polymer in excess. One limitation of this approach, however, is that if the T_g of one component overlaps with a signal from the other component, then it is not possible to extract information. Several other methods have been used to study interactions in polymer blends (Thomas et al. 2015): microscopy, light scattering, neutron scattering, rheology and different kinds of spectroscopic techniques, including Fourier-transform infrared spectroscopy and solid-state nuclear magnetic resonance. Among these techniques, positron annihilation lifetime spectroscopy (PALS) occupies a special place because it provides a method for examining and characterising the distribution of cavities at a molecular level, indicating the nature of the free volume in the analysed sample (Jean et al. 2013). PALS is a very flexible technique and its applications span from the investigation of defects in metals or semiconductors (Eldrup and Singh 1997) and the free volume in polymers (Pandini et al. 2017; Consolati et al. 2018) to the

distribution of nanoparticles inside polymer brushes (Panzarasa et al. 2016, 2017; Dehghani et al. 2018). As such, PALS has been used to investigate the free volume hole properties of both miscible and immiscible blends (Liu et al. 1995; Wästlund and Maurer 1997; Ramya et al. 2013).

Blends of ethyl cellulose (EC) and poly(vinylpyrrolidone) (PVP) are non-miscible and undergo phase separation upon solvent removal. This characteristic, combined with the good filmogenic properties of both polymers, is especially useful for the coating of medical formulations with controlled release of slightly hydrosoluble drugs (Mukherjee et al. 2005; Yang et al. 2014). For this purpose, microsegregated coatings are developed in which the ethyl cellulose provides mechanical stability while the PVP phase dissolves in aqueous solvents. Despite the industrial relevance of this kind of coatings, however, the study of their properties is still an open field of investigation (Chan et al. 2005; Kutsenko et al. 2013) and no reference is currently available for the study of EC-PVP blends with PALS. Only a few studies have been dedicated to the single polymers ethyl cellulose (Doyle, S.; Malhotra, B. D.; Peacock, N.; Pethrick 1984; Hegyesi et al. 2014) and PVP (Li et al. 2003; Shpotyuk et al. 2016) and none to their blends. The aim of this study is to fill such a gap, providing a novel understanding of such important blends by means of a combined thermo-mechanical analysis and PALS study.

Experimental section

Materials and methods

Ethyl cellulose (EC, Ethocel® Dow Chemicals; viscosity 15-25 mPa·s, ethoxyl content 48.0-49.5 %w/w, according to the producer), poly(vinyl pyrrolidone) (PVP, average M_w 10, 30, 40, 55 and 360 kDa, according to the producer) and absolute ethanol were purchased from Sigma-Aldrich and used as received. Films of pure polymers and blends were obtained by solution casting from ethanol solutions with a home-built bar-coating device on antiadhesive substrates (perfluorinated polymer). The parameters chosen were: set thickness 100 μm, deposition speed 11 mm s^{-1}. The films were dried at room temperature under a fume hood, detached from the support and stored in closed bags. The blend samples were named as "PVPn-EC x:y", where n indicates the average M_w of PVP while x and y are the mass ratios between PVP and EC.

Characterization

Attenuated total reflectance Fourier-transform infrared spectroscopy (ATR-FTIR) measurements were performed using a Nicolet iN10 (Thermo Fisher Scientific) with a diamond

optical window, scanning the spectral range 4000–600 cm^{-1} with a resolution of 4 cm^{-1}. Background (100 scans) was collected before each analysis (200 scans). Scanning electron microscopy (SEM) and energy dispersive X-ray spectroscopy (EDX) were performed with a Hitachi SU5000 FE-SEM. The samples were sputter-coated with 4 nm of Au-Pd alloy to make them conductive.

Differential scanning calorimetry (DSC) tests were carried out by means of a DSC Q100 (Thermal Analysis Inc.), employing nitrogen as purge gas. About 5-10 mg of the film was tested by the application of a thermal program, consisting in a first heating run at 10°C min^{-1} from –50°C to 225°C, followed by a cooling run at 10°C min^{-1} to –50°C and by a second heating run at 10°C min^{-1} to 225°C. The results were employed to evaluate the material glass transition temperature (as the inflection point on the second heating scan) and the melting temperature (as maximum of the endothermal peak in the second heating scan). All the materials (PVP 360; EC; the blends obtained with PVPn-EC in the ratios 1:1, 1:4, 1:8, where n = 360, 55, 40, 30 and 10 kDa) were tested in their as-produced state. Only few materials (pure EC; pure PVP360; blend PVP40-EC 1:1; blend PVP40-EC 1:4; blend PVP40-EC 1:8) were tested after a thermal treatment at 150°C for 6 h under vacuum to remove the possible presence of water.

Dynamic-mechanical thermal analysis (DMTA) was performed by means of a DMA Q800 (Thermal Analysis Inc.) under tensile configuration on rectangular strips (overall length: 25 mm; length between grips: 15 mm; width: 5 mm; thickness: about 0.1 mm). The strips were cut out from the cast sheets by means of a sharp cutter, in regions where the cast films present the most homogeneous thickness and a reduced presence of defects. The tests were performed under displacement control, employing a displacement amplitude of 15 μm at 1 Hz and a thermal ramp between room temperature and 200°C at 3°C min^{-1}.

PALS measurements were carried out on samples obtained by cutting small pieces from the same batch. They were stacked to reach a thickness (2 mm) enough to stop all the injected positrons. Positron were emitted from a ^{22}Na source. This was enveloped between two Kapton® foils (thickness 7.6 μm each) which were glued to each other; the whole was placed between two identical samples in a typical ‘sandwich’ configuration. Positron annihilation lifetime spectra were collected through a conventional fast–fast coincidence setup, having a resolution of about 300 ps. Each spectrum, containing about $4 \cdot 10^6$ counts, was analyzed through the computer program LT (Kansy 1996), with a suitable correction for the positrons annihilated in Kapton. For each temperature value were collected three spectra. Both non-dry and dry samples were measured, as discussed before.

Results and discussion

153 Morphological characterization

154 The cross-sections of all samples were analyzed by scanning electron microscopy (SEM).
155 That the two polymers are not interacting *i.e.* they are immiscible is visible in the SEM images
156 (Figure 1), where discoidal structures can be easily distinguished from an embedding matrix. Such a
157 morphology is indicative of phase separation, and the size of the discoids seems to increase for PVP
158 of increasing molecular weight, but it is difficult to draw more conclusions based on SEM images
159 alone.

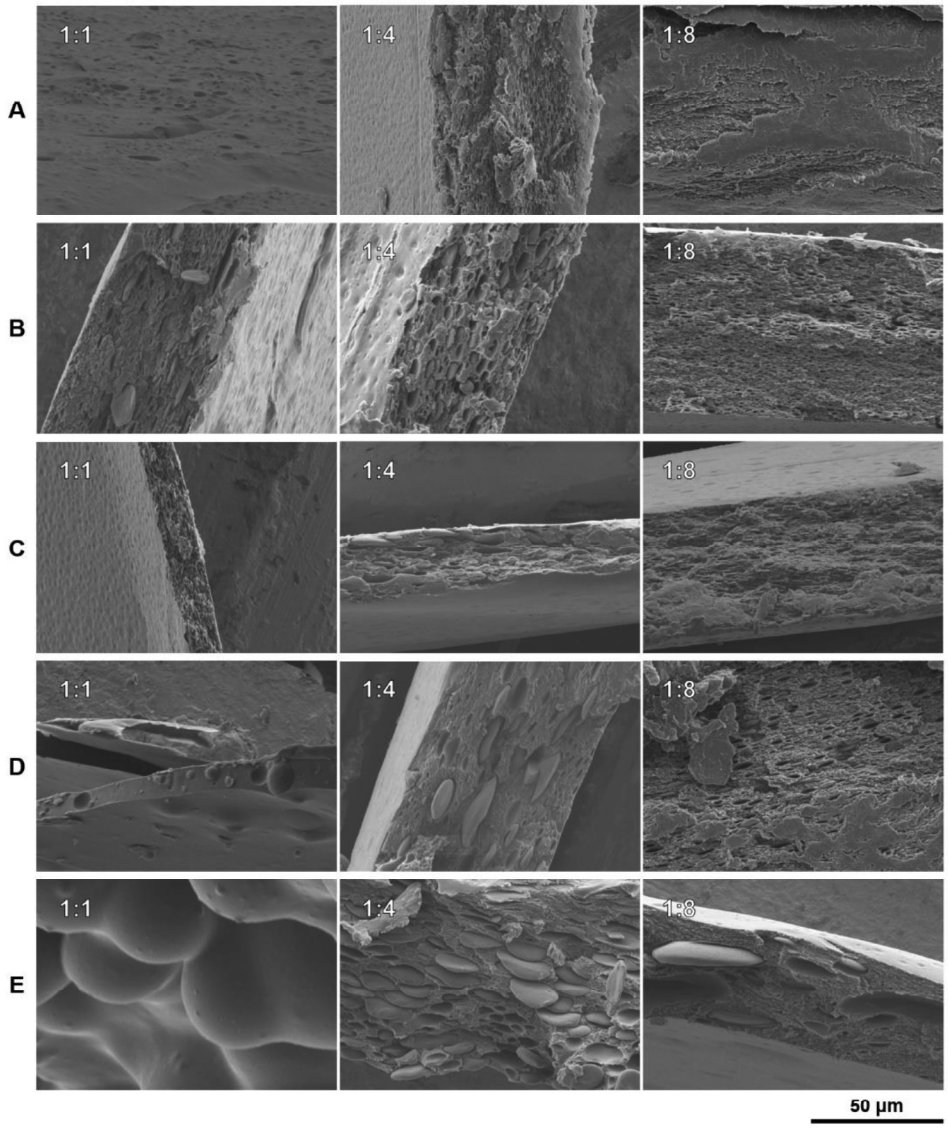

160

161 **Fig. 1** SEM images of the blend films (cross-section). The PVP:EC mass ratio is indicated for each
162 image. a) Blends with PVP10; b) blends with PVP30; c) blends with PVP40; d) blends with PVP55;
163 e) blends with PVP360.

164

Energy-dispersive X-ray spectroscopy (EDX) analysis was used to investigate the elemental composition of these two different phases: the results obtained for the blend PVP360-EC 1:4 are summarized in Table 1. This sample was chosen as the most representative one because of the nice separation observed between the matrix and the discoidal structures. These latter appear to be made of a mixture of PVP and EC, while the surrounding matrix, which apparently does not contain nitrogen, should consist mainly of EC.

Table 1. Elemental composition, according to EDX, of the structures observed in the PVP360-EC 1:4 blend sample.

Structure investigated	Elemental composition (atom%)			Elemental ratios	
	C	N	O	C/N[a]	C/O[b]
Discoid	60.93	17.35	21.72	3.5	2.8
Matrix	72.95	-	27.05	0	2.7

[a]Theoretical: for pure PVP, 6; for pure EC, 0. [b]Theoretical: for pure PVP, 6; for pure EC, ≈5.

Fourier-transform infrared spectroscopy (FTIR) is one method of choice to probe the nature and extent of interactions in polymer blends. The reason behind is that the mixing of two components at the molecular level will cause changes in the molecules' oscillating dipoles. This, in turn, will manifest itself as changes in the frequency and bandwidth of the interacting groups in the spectrum. If the two polymers interact, then their functional groups will show band shifts and broadening compared to the spectra of the pure polymers (Nair et al. 2001; Silverstein M.Robert, Webster X. Francis 2005).

In principle, PVP is capable of hydrogen bonding through both the nitrogen atom or the carbonyl group on the pyrrole ring. However, steric hindrance precludes the involvement of nitrogen atom in intermolecular interactions, thus making the carbonyl group more favorable for hydrogen bonding. In the case of a blend of PVP and EC, one could expect hydrogen bond interactions to take place *e.g.* between the C=O of PVP and the free –OH groups of EC. The FTIR spectra of the different investigated polymer blends are shown in Figure S1. No significant shift of the 1650 cm^{-1} carbonyl peak of PVP could be observed, independently of the molecular weight of the latter. The blends thus gave spectra which are the sum of those of EC (Hegyesi et al. 2013) and PVP, suggesting the

absence of interactions between the two polymers and thus the non-miscibility of the studied blends.

Differential scanning calorimetry (DSC)

Analyzed as-produced by differential scanning calorimetry (DSC) the samples displayed, on the first heating scan, endothermal signals with different intensities and positions depending on the type of analyzed polymer. As an example, the DSC traces of the pure polymers, PVP360 and EC, are reported in Figure 2a and Figure 2b, respectively.

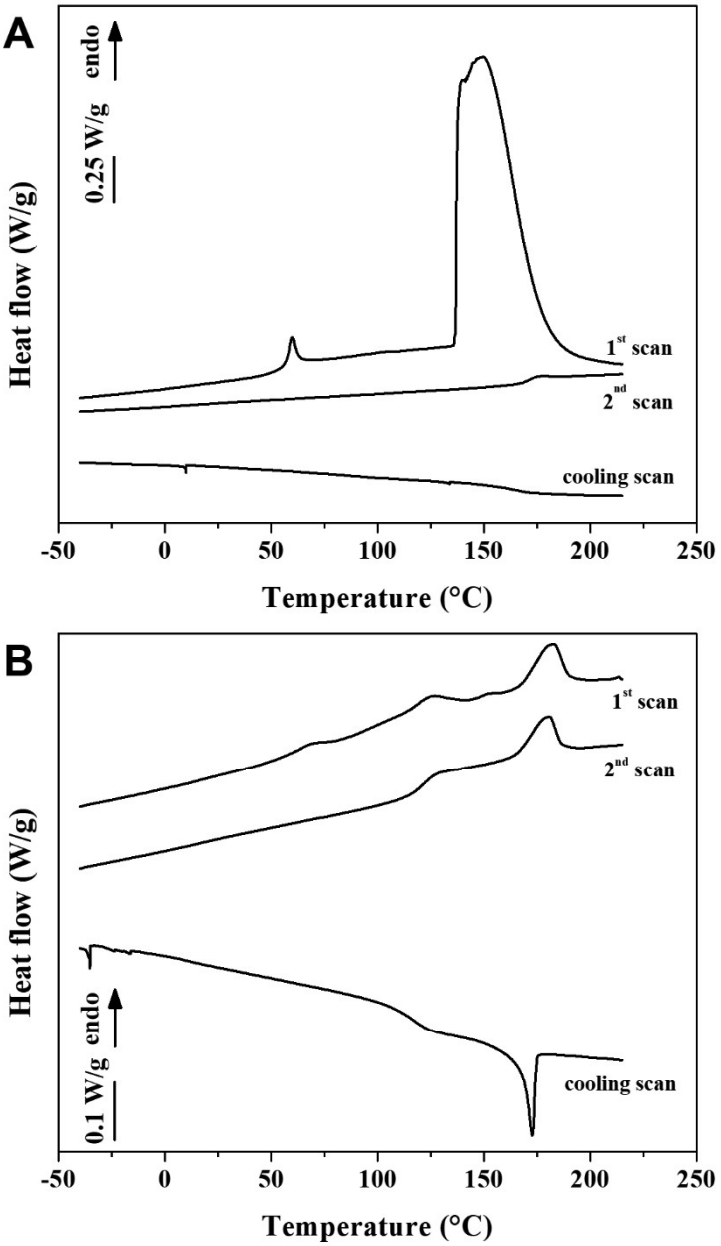

Fig. 2 DSC results of the 1st, 2nd and cooling scan for a) PVP360 and b) EC.

The 1st heating scan of PVP360 displays a large endothermal peak between 140°C and 200°C and a less prominent one at 50°C, which are both absent in the 2nd heating scan. The 1st heating scan of EC displays two moderate endothermal peaks at 50°C and at 120°C, both absent in the 2nd scan, which features only the melting peak at 170°C. Such irreversible endothermal peaks observed for temperatures >100°C are suspected to be due to the presence in the samples of bound residual water. The 2nd heating scans, on the other hand, display for PVP360 only the inflection close to 170°C correlated to T_g while for EC both a defined inflection at about 120°C and a melting peak around 170°C are visible.

To determine the possible influence of residual water on samples' behavior, a selected set of samples was heated to 150°C for 6h under vacuum. This treatment allowed to extract water while avoiding the melting of EC crystalline phase. From the obtained results (reported as example in Figure S2) it is possible to conclude the following: i) by comparing the 1st heating scan of the as-cast and the dried samples, it appears that water has been only partially removed; ii) no differences could be found between the 2nd heating scan of the as-cast and treated systems. These results suggest that the 2nd scan traces describe the glass transition and melting temperatures of the studied samples independently of their history. Eventually, DSC analyses were carried out on the as-produced films and the results evaluated on the 2nd scan traces. Representative 2nd heating scans of PVP360, EC and their blends are shown in Figure 3.

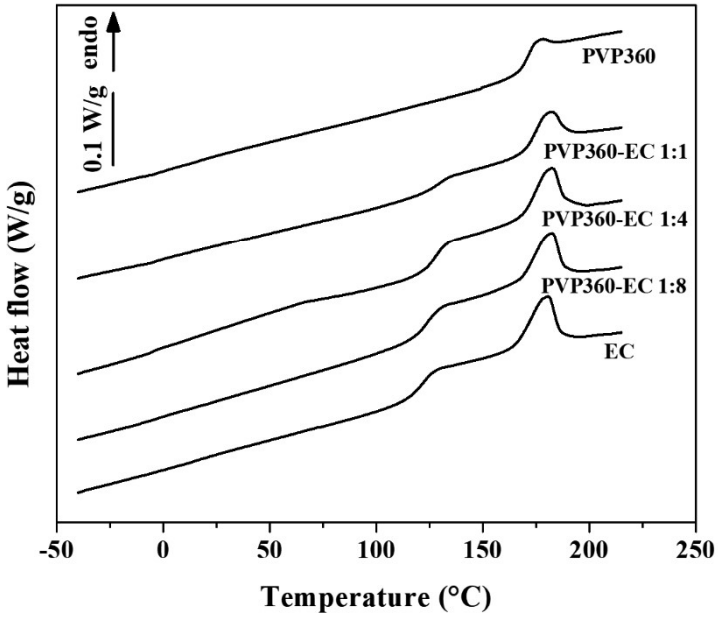

Fig. 3 DSC results (2nd heating scan) for PVP360, EC, and their blends.

The DSC traces clearly show, for all systems, the glass transition region and (except for pure PVP) the melting region. For PVP360 a glass transition at about 170°C can be measured and no crystalline phase is found, while EC displays a glass transition at about 120°C and a melting temperature close to 170°C *i.e.* in correspondence to the T_g of PVP360. The three blends analyzed display intermediate values of T_g with respect to EC and PVP360, mainly located close to those of EC, and being closer to this value the higher the EC content. In addition, the extent of the inflection on the curves seems to become less marked as the EC content decreases, which suggests a governing role of EC on the measured T_g. The crystallization peak is present in all the blends, showing that the crystallization is not suppressed. Its area, which represents the melting enthalpy, has values mostly scaled with the EC content for the mixing ratios 1:8 and 1:4, suggesting that the specific crystallinity per EC content remains the same, while for the mixing ratios 1:1 the specific crystallinity percent per EC content is 20%-30% higher than expected. The melting of EC occurs in the same region in which PVP360 shows its glass transition, thus masking another possible glass transition whose presence could provide information on the systems' miscibility. Similar results were obtained for the other systems, which gave traces closely resembling those of Figure 3 with evident glass transition and melting events. The values of T_g, T_m and of the melting enthalpy ΔH_m are reported in Table 2 and Table 3.

Table 2 Glass transition temperature T_g and melting temperature T_m (parentheses) determined by DSC on the 2nd heating scan of the various materials tested as-produced.

		Mixing ratio PVP:EC		
Sample	pure polymer	1:1	1:4	1:8
PVP360	171 °C (-)	-	-	-
PVP360-EC	-	130 °C (181 °C)	127 °C (182 °C)	124 °C (182 °C)
PVP55-EC	-	128 °C (182 °C)	128 °C (180 °C)	129 °C (182 °C)
PVP40-EC	-	126 °C (177 °C)	128 °C (181 °C)	126 °C (181 °C)
PVP55-EC	-	128 °C (180 °C)	124 °C (180 °C)	130 °C (181 °C)
PVP10-EC	-	117 °C (177 °C)	122 °C (179 °C)	121 °C (179 °C)
EC	122 °C (180 °C)	-	-	-

Table 3 Melting enthalpy ΔH_m determined by DSC from the 2nd heating scan of the various samples tested as-produced.

		Mixing ratio PVP:EC		
Sample	pure polymer	1:1	1:4	1:8
PVP360	-	-	-	-
PVP360-EC	-	3.7 Jg^{-1}	5.6 Jg^{-1}	5.3 Jg^{-1}
PVP55-EC	-	4.2 Jg^{-1}	4.5 Jg^{-1}	4.9 Jg^{-1}
PVP40-EC	-	3.4 Jg^{-1}	4.7 Jg^{-1}	5.4 Jg^{-1}
PVP55-EC	-	3.6 Jg^{-1}	3.8 Jg^{-1}	4.3 Jg^{-1}
PVP10-EC	-	2.6 Jg^{-1}	3.8 Jg^{-1}	4.9 Jg^{-1}
EC	5.5 Jg^{-1}	-	-	-

The values of T_g show only a slight dependence on the polymer mixing ratios for the samples based on PVP55, PVP40 and PVP30, while, for samples obtained with PVP10, even lower values of T_g were obtained, such as for blend with 1:1 mixing ratio, suggesting a weak plasticizing effect ascribed to the low molecular weight PVP10. The slight dependence of the T_g on the polymer ratio is interpreted as the absence of a proper mixing between the two polymers. In Figure 4 the T_g of the various samples are displayed as a function of the mixing ratio and compared to the theoretical T_g values expected for ideal mixing, according to the Fox equation (eq. 1):

$$1/T_g = (w_{PVP360} / T_{g,PVP360}) + (w_{EC} / T_{g,EC}) \quad (1)$$

where w_{PVP360} and w_{EC} represent the weight fractions of the two polymers, while $T_{g\,PVP360}$ and $T_{g,EC}$ are the T_g of the polymers expressed as absolute temperatures. As can be seen from Figure 4, the experimental data for almost all the investigated compositions display a downward deviation from the values corresponding to the curve of ideal miscibility.

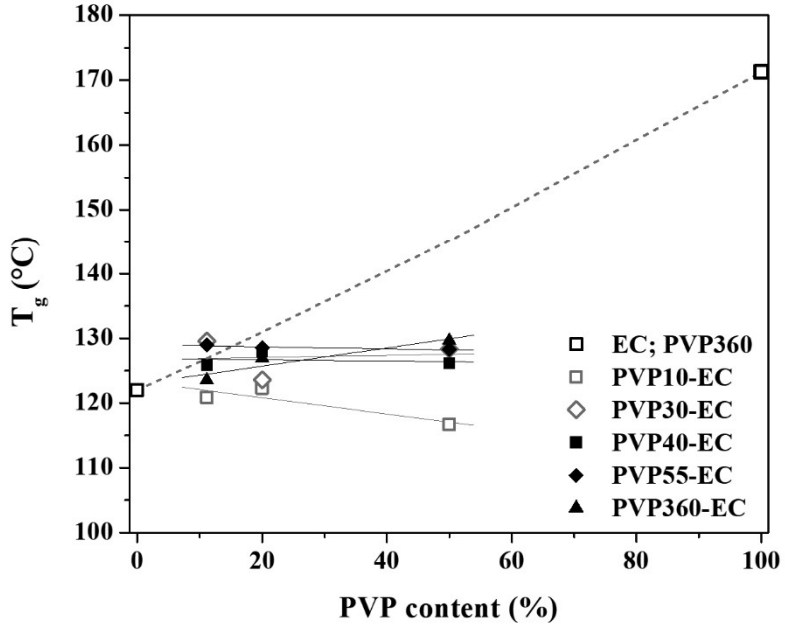

Fig. 4 T_g values of the various systems as a function of the PVP content and representation of the Fox equation for complete miscibility of the two polymers EC and PVP.

Dynamic-mechanical thermal analysis (DMTA)

Dynamic-mechanical thermal analysis was carried out on the various materials with the aim to evaluate the mechanical response of the systems and its dependence on temperature.

The results are reported as E' traces: Figure 5a shows those for PVP360 and EC while Figure 5b those for representative blends, namely those obtained by mixing PVP360 and EC with different ratios. The curves obtained for the pure polymers show that PVP is characterized by a higher stiffness (about twice) than that of EC and by a higher glass transition temperature, at which the modulus decreases and rapidly approaches the flow regime. By contrast, EC presents a first moderate modulus reduction at lower temperatures.

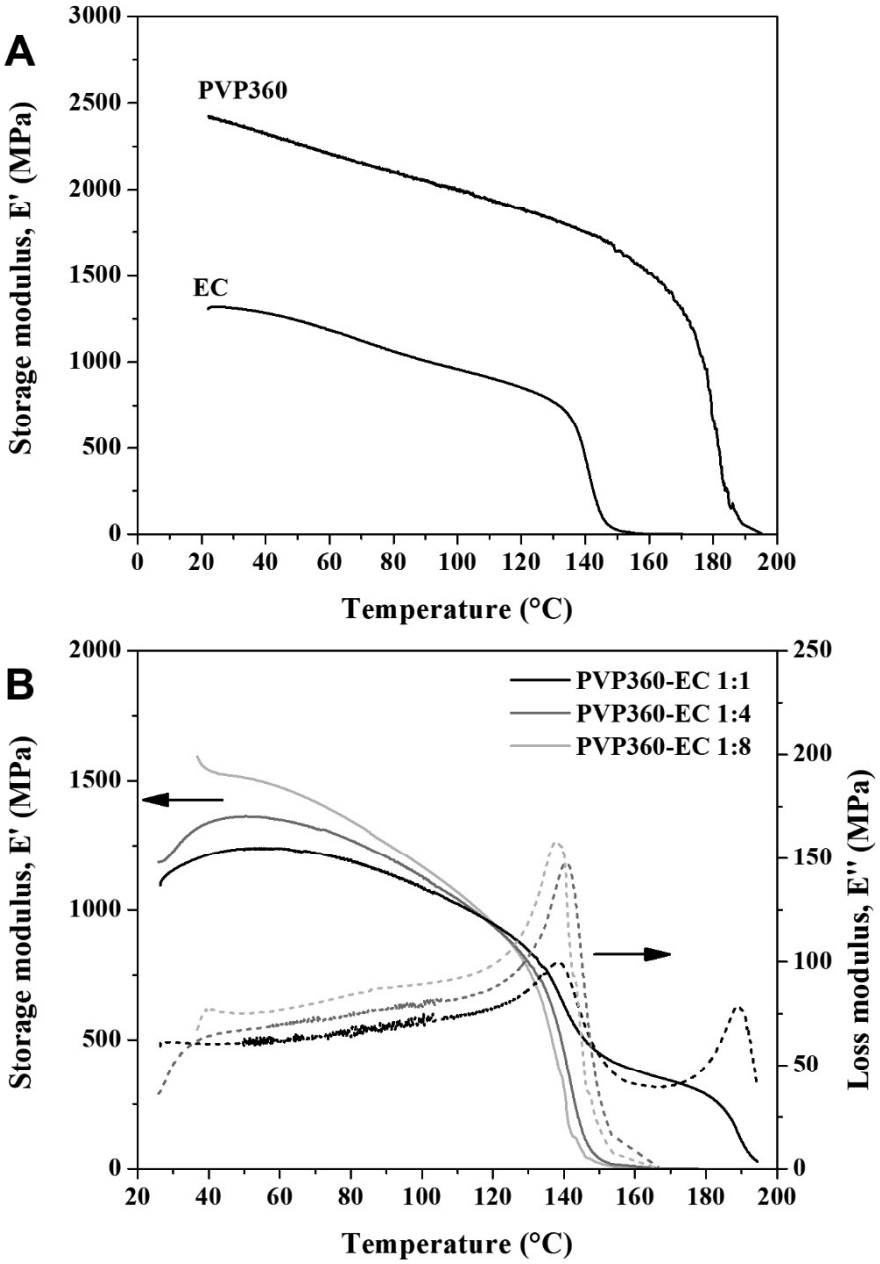

Fig. 5 Storage modulus traces of a) PVP 360 and EC; b) Storage modulus (solid lines) and loss modulus (dashed lines) for the blends PVP360-EC 1:x with x = 1, 4, 8.

The polymer blends show limited differences in the modulus values, with values in the glassy region very close to that of EC. The blend stiffness is strongly determined by EC: blends with high EC contents (PVP360-EC 1:4 and PVP360-EC 1:8) display a modulus drop that rapidly lead to entrance in the flow region; only the system PVP360-EC 1:1 presents an extension of the material solid behavior above the T_g of EC.

By comparing all the E' traces obtained, it appears that only the samples obtained by mixing to PVP360 and EC in equal amounts (1:1) present such extension in terms of a rubber plateau from T_g to the melting region of EC. This behavior is in contrast with that of the other samples, which, independently of the PVP molecular weight and the PVP:EC mixing ratios, display a faster decrease in correspondence of the T_g of EC, as it can be seen in Figure 6a-c. These results suggest that only in presence of the maximum amount of PVP with the highest molecular weight tested (360 kDa), the co-continuous structure obtained could still provide mechanical stiffness after EC has undergone glass transition. By contrast, lower amounts of PVP360 would lead to flow, since an effective PVP co-continuous structure is not obtained, and so does any content of PVP with lower molecular weight.

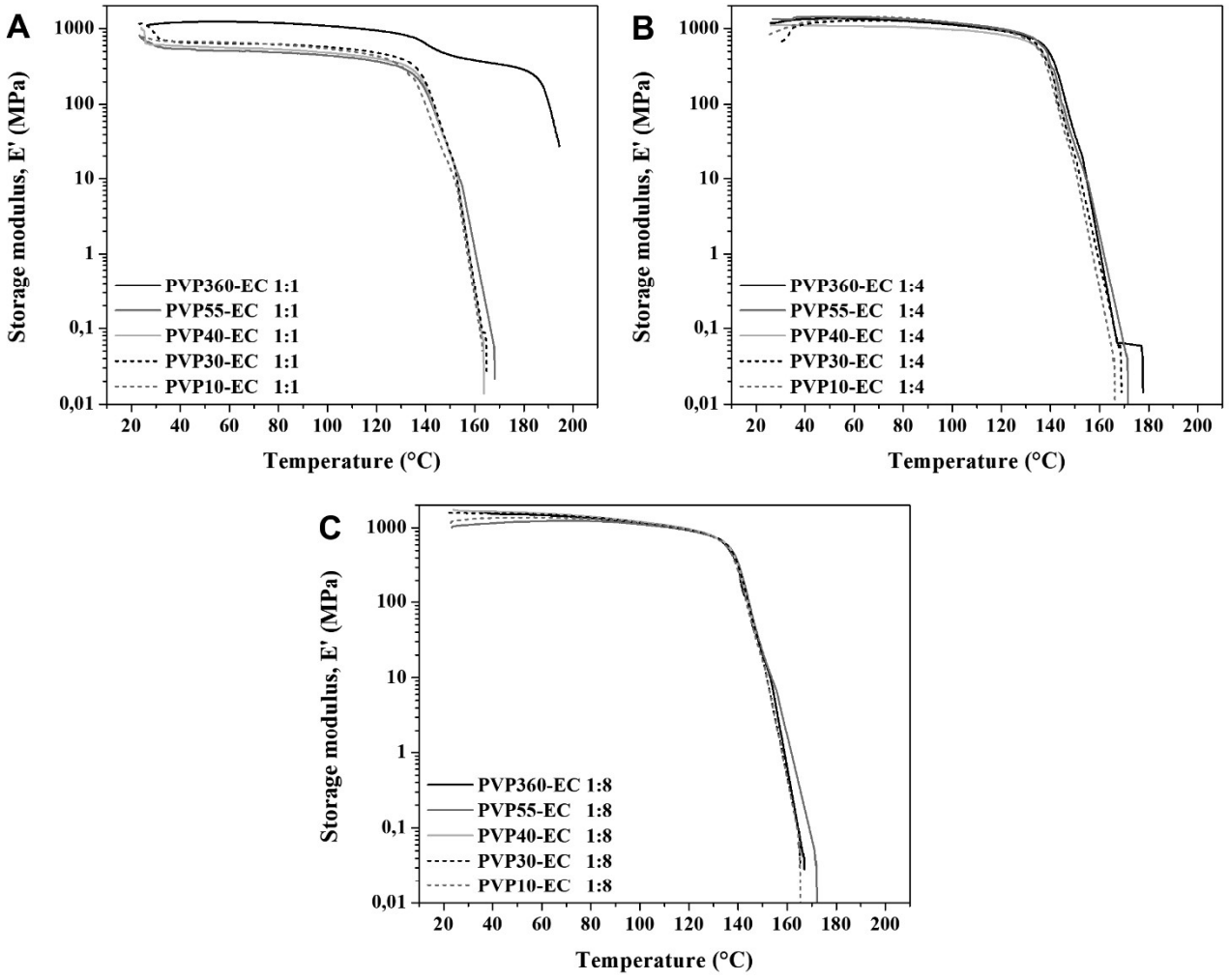

Fig. 6 Storage modulus traces of the blends based on EC and on PVP with various molecular weights obtained for mixing ratios equal to a) 1:1, b) 1:4, and c) 1:8.

To describe the effects of the material composition, both stiffness and T_g of the various systems were evaluated: the results are reported as a function of the PVP content in Figure 7. The stiffness was evaluated at 40°C, i.e. well below T_g, while T_g was evaluated in correspondence to the E'' peak temperature. The results show that the modulus decreases with the PVP content, except for the PVP360 sample, the modulus of which is above that of EC. For PVP of lower molecular mass the modulus remains close or slightly higher than EC for samples obtained with PVP:EC ratios of 1:8 and 1:4. An important decrease is observed for the 1:1 mixing ratio, suggesting a possible plasticization due to the low molecular weight PVP. The results obtained for T_g confirm and highlight what already discussed, for the DSC results, on the non-miscibility of the two polymers.

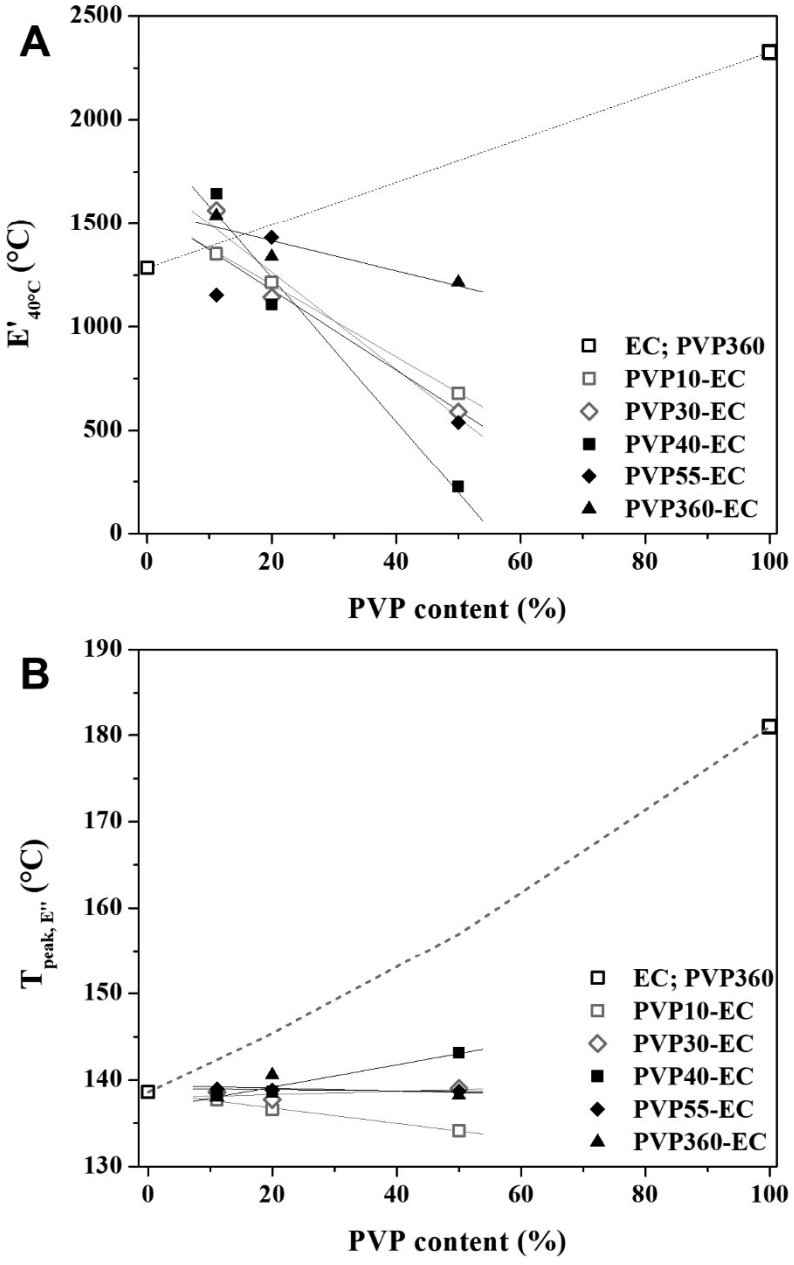

Fig. 7 a) Storage modulus values at 40°C and b) T_g values of the various systems as a function of the PVP content; in b) the dashed line represents the Fox equation for complete miscibility of the two polymers.

Positron annihilation lifetime spectroscopy (PALS)

Positron annihilation lifetime spectra were successfully analysed in three components, a common situation found in polymer investigations. The normalized χ^2 gave values in the range 0.96 – 1.07. The shortest lifetime component is attributed to positrons annihilating in the bulk as well as to para-Ps annihilations (the ground state sublevel with antiparallel spins). This last contribution cannot be resolved as a distinct component, owing to both the resolution of the apparatus and the faint intensity of the signal, which is expected to be of the order of one third of the intensity of the longest lifetime component. The intermediate component originates from positrons annihilating into defects and free volume holes. The lifetime of this component is higher than the shortest one since the electron density surrounding the positron is lower with respect to the bulk. The longest component is due to the annihilation of ortho-positronium atom (o-Ps, the ground state sublevel with parallel spins) into the holes present in the amorphous zones. Therefore, such a component is used to probe the free-volume hole dimensions. This is possible thanks to a correlation between o-Ps lifetime and the size of the cavity, which can be cast in a quantitative form by suitably modeling the trapping site. Indeed, a longer o-Ps lifetime is found in bigger holes, since the lower electron density surrounding Ps reduces the probability of Ps annihilation. Cavities show a distribution of sizes, owing to the disordered character of the amorphous zone. This involves a distribution of o-Ps lifetimes, which can be obtained from the analysis of annihilation lifetime spectra.

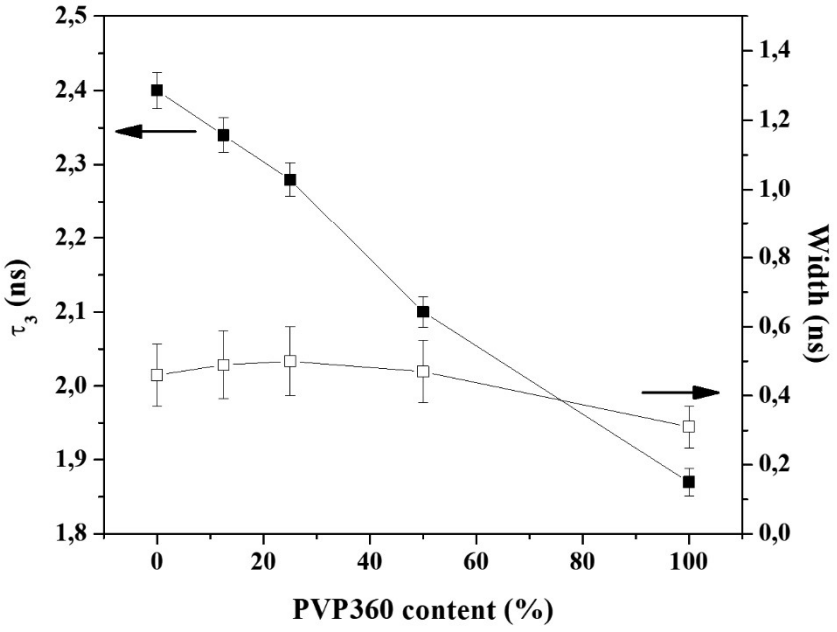

Fig. 8 Evolution of positronium lifetime τ_3 and of the width of lifetime distribution for increasing PVP360 content.

According to thermo-mechanical analysis, the samples based on PVP360 were found to give the most interesting results. For this reason, Figure 8 and Figure 9a show the data obtained by means of PALS only for the pure EC and PVP360 as well as for the related blends. Only Figure 9b features the comparison of the values of the relative free volume fraction *f* as a function of PVP molecular weight. All the other PALS results are displayed in the Supporting Information (Figure S3). The results obtained for the pure polymers are in accordance with previous literature reports. The lifetime τ_3 measured for ethyl cellulose is 2.40 ns, comparable with the 2.32 ns reported for commercial Ethocel 45 (Hegyesi et al. 2014); for PVP360, the literature measurements indicate τ_3 = 1.86 ns (measured for PVP40) (Shpotyuk et al. 2016), in perfect agreement with our measured value of 1.87 ns. The centroid of the o-Ps lifetime distribution decreases monotonically on increasing the content of PVP360, as can be expected by considering the remarkable difference of lifetimes in the two pure polymers. It is possible to translate the lifetime values into cavity sizes by using the simplest model, the Tao-Eldrup equation (Tao 1972; Eldrup et al. 1981), which considers spherical holes and it has been successfully used in many PALS investigations. Due to a monotonic, although nonlinear, relationship between o-Ps lifetime (shown in Figure 8) and the corresponding radius of the host cavity, we can interpret the τ_3 results in terms of decreasing average radius of free volume holes. Figure 8 shows also the width of lifetime distribution, which decreases on passing from blends to pure PVP360.

349 The behavior of Ps formation is very different for the two investigated polymers. Its formation is
350 especially favored in pure EC, as demonstrated by data in Figure 9a where the o-Ps intensity is
351 shown versus the PVP360 content. This could be due to the polar character of PVP: indeed, the
352 carbonyl group attracts the positron, with consequent annihilation; the probability of Ps formation is
353 therefore reduced, as observed. Using an empirical approach (Wang et al. 1990), quite common in
354 this kind of investigations, we can estimate a relative free volume fraction f by taking the product
355 of the average volume of the cavities, v_h, times the o-Ps intensity I_3, which is assumed to depend on
356 the number density of free volume holes (although other phenomena related to the chemistry of Ps
357 in the material can influence its formation) (eq. 2):

358 $$f = v_h I_3 \quad (2)$$

359 As shown in Figure 9b, the behavior of f is quite reminiscent of that of o-Ps lifetime, the parameter
360 with the largest variation as a function of PVP360 content.

361

362

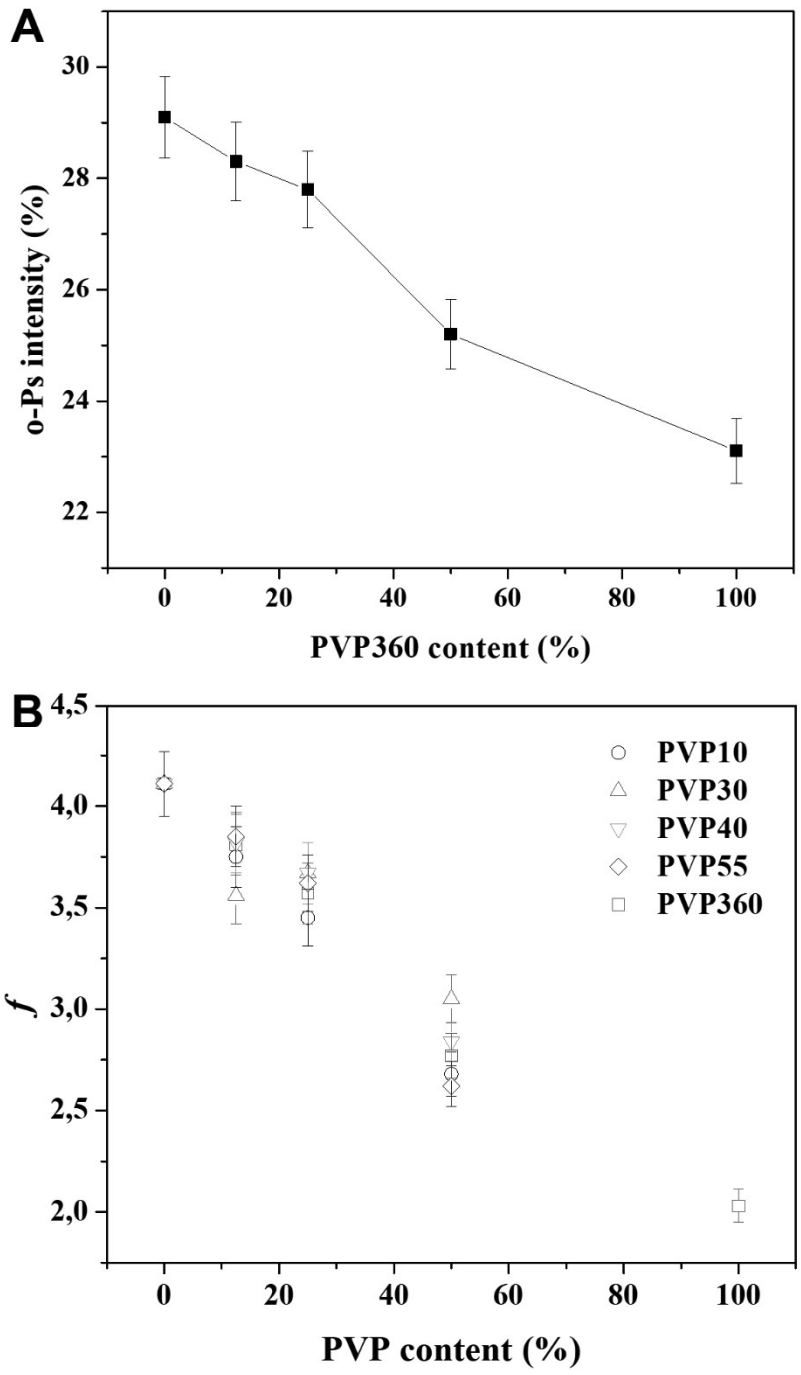

Fig. 9 a) Intensity of o-Ps and b) evolution of *f* parameter as a function of PVP360 content of the blends.

Conclusions

In the present work we investigated the morphology, thermomechanical properties and the free volume of two polymers, ethyl cellulose and poly(vinyl pyrrolidone), and of their immiscible blends.

The absence of interactions between the two polymers was revealed by means of FTIR. Their immiscibility was further confirmed by morphological analysis and the behavior of the glass transition temperature.

Dynamic-mechanical thermal analyses pointed out that mechanical stiffness of the blends in the temperature range above the T_g of EC can be granted only in the case of the highest content of PVP with the highest molecular weight.

PALS results showed that o-Ps lifetime, and consequently the average size of the free volume holes, increases with the content of EC in the blends. Analogous behavior is displayed by o-Ps intensity, which may be correlated to the number density of holes. Moreover, PVP displays a more ordered distribution of cavity sizes, as shown by a narrower o-Ps lifetime distribution.

The combined effects of average sizes, distribution and number density of holes determine an increased free volume in all the investigated structures when the amount of EC increases.

Since the free volume is a primary parameter affecting permeability and transport properties of coatings and films, the results here discussed will be useful for applications of EC-PVP blends in which controlled release and filtering of small molecules is required.

Electronic supplementary material

The online version of this article contains supplementary material, which is available to authorized users.

References

Barlow JW, Paul DR (1981) Polymer blends and alloys—a review of selected considerations. Polym Eng Sci. 21:985-996. doi: 10.1002/pen.760211502

Brostow W, Chiu R, Kalogeras IM, Vassilikou-Dova A (2008) Prediction of glass transition temperatures: Binary blends and copolymers. Mater Lett. 62:3152. doi: 10.1016/j.matlet.2008.02.008

401 Chan LW, Ong KT, Heng PWS (2005) Novel film modifiers to alter the physical properties of
402 composite ethylcellulose films. Pharm Res 22:476–489. doi: 10.1007/s11095-004-1886-7

403 Consolati G, Panzarasa G, Quasso F (2018) Morphology of free volume holes in an amorphous
404 polyether-polyester polyurethane of biomedical interest. Polym. Test. 68:208-212. doi:
405 10.1016/j.polymertesting.2018.04.016

406 Dehghani ES, Aghion S, Anwand W, et al (2018) Investigating the structure of crosslinked polymer
407 brushes (brush-gels) by means of Positron Annihilation Spectroscopy. Eur Polym J. 99:415-
408 421. doi: 10.1016/j.eurpolymj.2017.12.042

409 Doyle, S.; Malhotra, B. D.; Peacock, N.; Pethrick RA (1984) Positron Annihilation and X-ray
410 Diffraction Studies of Cellulose and some Derivatives. Brit Polym J 16:15–20

411 Eldrup M, Lightbody D, Sherwood JN (1981) The temperature dependence of positron lifetimes in
412 solid pivalic acid. J. Chem. Phys. 63:51-58. doi: 10.1016/0301-0104(81)80307-2

413 Eldrup M, Singh BN (1997) Studies of defects and defect agglomerates by positron annihilation
414 spectroscopy. J Nucl Mater. 251:132-138. doi: 10.1016/S0022-3115(97)00221-3

415 Hegyesi D, Sovány T, Berkesi O, et al (2013) Study of the effect of plasticizer on the structure and
416 surface characteristics of ethylcellulose free films with FT-IR spectroscopy. Microchem J
417 110:36–39. doi: 10.1016/j.microc.2013.02.005

418 Hegyesi D, Süvegh K, Kelemen A, et al (2014) Characterization of ethylcellulose free films by
419 positron annihilation spectroscopy and mechanical testing. Microchem J 115:47–50. doi:
420 10.1016/j.microc.2014.02.007

421 Imre B, Pukánszky B (2013) Compatibilization in bio-based and biodegradable polymer blends.
422 Eur. Polym. J. 49:1215-1233.

423 Jean YC, Van Horn JD, Hung WS, Lee KR (2013) Perspective of positron annihilation
424 spectroscopy in polymers. Macromolecules 46:7133–7145. doi: 10.1021/ma401309x

425 Kansy J (1996) Microcomputer program for analysis of positron annihilation lifetime spectra. Nucl
426 Instruments Methods Phys Res Sect A Accel Spectrometers, Detect Assoc Equip 374:235–244.
427 doi: 10.1016/0168-9002(96)00075-7

428 Kutsenko LI, Santuryan YG, Kalyuzhnaya LM, et al (2013) Properties of solutions and films of
429 blends of ethyl cellulose with polyvinylpyrrolidone and Poviargol. Russ J Appl Chem 86:558–
430 563. doi: 10.1134/S1070427213040186

431 Li Y, Zhang R, Chen H, et al (2003) Depth profile of free volume in a mixture and copolymers of
432 poly(N-vinyl-pyrrolidone) and poly(ethylene glycol) studied by positron annihilation
433 spectroscopy. Biomacromolecules 4:1856–1864. doi: 10.1021/bm034292i

434 Liu J, Jean YC, Yang H (1995) Free-Volume Hole Properties of Polymer Blends Probed by
435 Positron Annihilation Spectroscopy: Miscibility. Macromolecules 28:5774–5779. doi:
436 10.1021/ma00121a012

437 Mukherjee B, Mahapatra S, Gupta R, et al (2005) A comparison between povidone-ethylcellulose
438 and povidone-eudragit transdermal dexamethasone matrix patches based on in vitro skin
439 permeation. Eur J Pharm Biopharm 59:475–483. doi: 10.1016/j.ejpb.2004.09.009

440 Nair R, Nyamweya N, Gönen S, et al (2001) Influence of various drugs on the glass transition
441 temperature of poly(vinylpyrrolidone): a thermodynamic and spectroscopic investigation. Int J
442 Pharm 225:83–96. doi: 10.1016/S0378-5173(01)00767-0

Pandini S, Bignotti F, Baldi F, et al (2017) Thermomechanical and large deformation behaviors of antiplasticized epoxy resins: Effect of material formulation and network architecture. Polym Eng Sci. doi: 10.1002/pen.24555

Panzarasa G, Aghion S, Marra G, et al (2017) Probing the Impact of the Initiator Layer on Grafted-from Polymer Brushes: A Positron Annihilation Spectroscopy Study. Macromolecules 50:5574-5581. doi: 10.1021/acs.macromol.7b00953

Panzarasa G, Aghion S, Soliveri G, et al (2016) Positron annihilation spectroscopy: A new frontier for understanding nanoparticle-loaded polymer brushes. Nanotechnology 27:02LT03. doi: 10.1088/0957-4484/27/2/02LT03

Pernot H, Baumert M, Court F, Leibler L (2002) Design and properties of co-continuous nanostructured polymers by reactive blending. Nat Mater. 1:54–58. doi: 10.1038/nmat711

Ramya P, Meghala D, Pasang T, et al (2013) Interface profile studies in immiscible and partially miscible binary polymer blends from free volume measurement. J.Phys. Conf. Ser.443:012048. doi: 10.1088/1742-6596/443/1/012048

Robeson LM (2007) Polymer Blends: A Comprehensive Review: Chapter 2. Fundamentals of Polymer Blends. Polym Blends. doi: 10.3139/9783446436503

Shpotyuk O, Bujňáková Z, Baláž P, et al (2016) Positron annihilation lifetime study of polyvinylpyrrolidone for nanoparticle-stabilizing pharmaceuticals. J Pharm Biomed Anal 117:419–425. doi: 10.1016/j.jpba.2015.09.030

Silverstein M.Robert, Webster X. Francis KJD (2005) Spectrometric Identification of Organic Compounds; John Wiley & Sons, 7th revised edition.

Tao SJ (1972) Positronium annihilation in molecular substances. J. Chem. Phys. 56:5499–5510. doi: 10.1063/1.1677067

Thomas S, Grohens Y, Parameswaranpillai J (eds) (2015) Characterization of Polymer Blends. Wiley- VCH Verlag GmbH & Co.

Utracki LA (1989) Polymer alloys and blends. pp. 1–20. Hanser Publisher, Munich Wang YY, Nakanishi H, Jean YC, Sandreczki TC (1990) Positron annihilation in amine- cured epoxy polymers—pressure dependence. J. Polym. Sci. Part B Polym. Phys. 28:1431-1441. doi: 10.1002/polb.1990.090280902

Wästlund C, Maurer FHJ (1997) Positron lifetime distributions and free volume parameters of PEO/PMMA blends determined with the maximum entropy method. Macromolecules 30:5870–5876. doi: 10.1021/ma961604j

Yang M, Xie S, Li Q, et al (2014) Effects of polyvinylpyrrolidone both as a binder and pore-former on the release of sparingly water-soluble topiramate from ethylcellulose coated pellets. Int J Pharm 465:187–196. doi: 10.1016/j.ijpharm.2014.02.021

Figure

Click here to access/download;Figure;Figure 1.tif

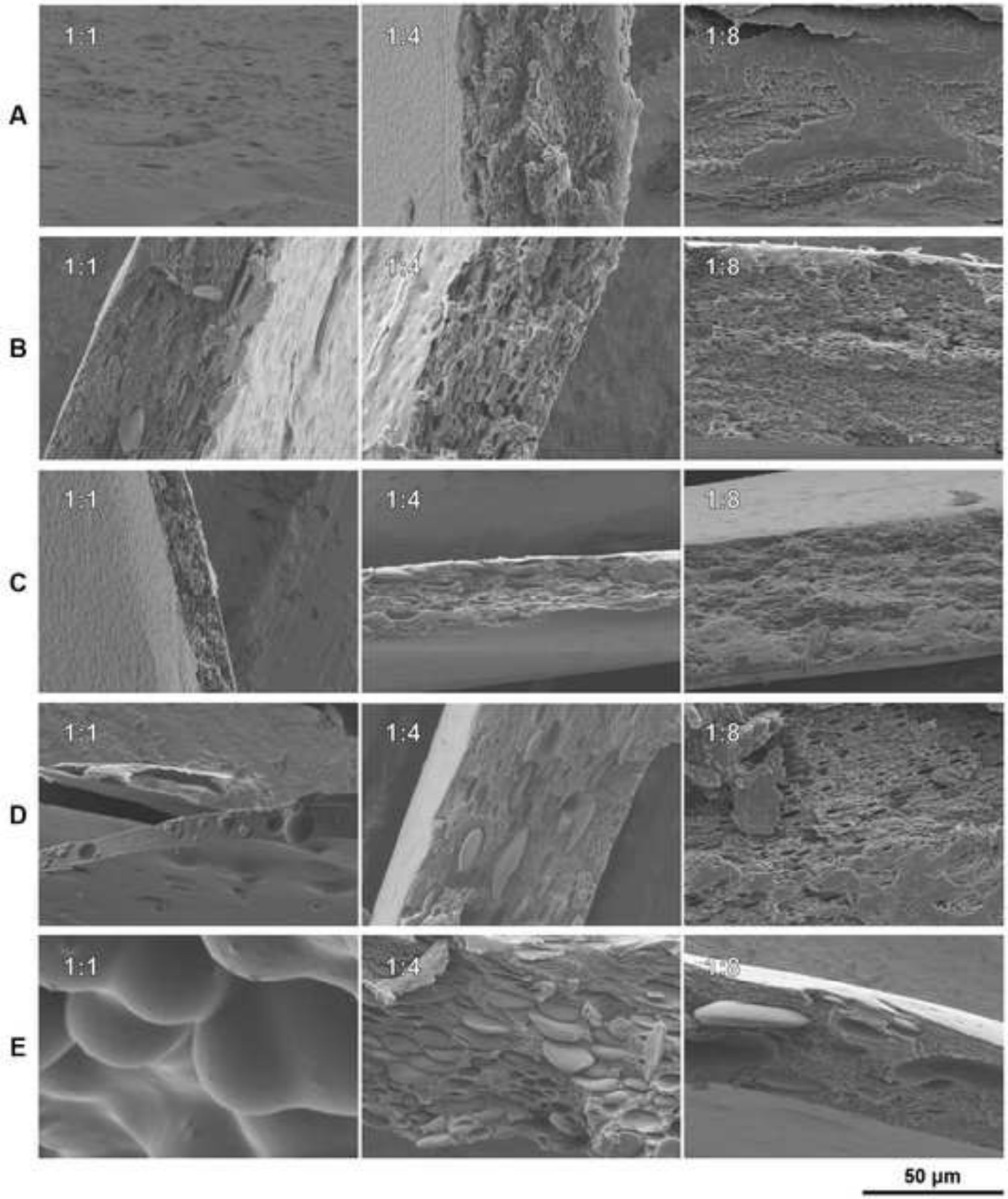

Figure

Click here to access/download;Figure;Figure 2.tif

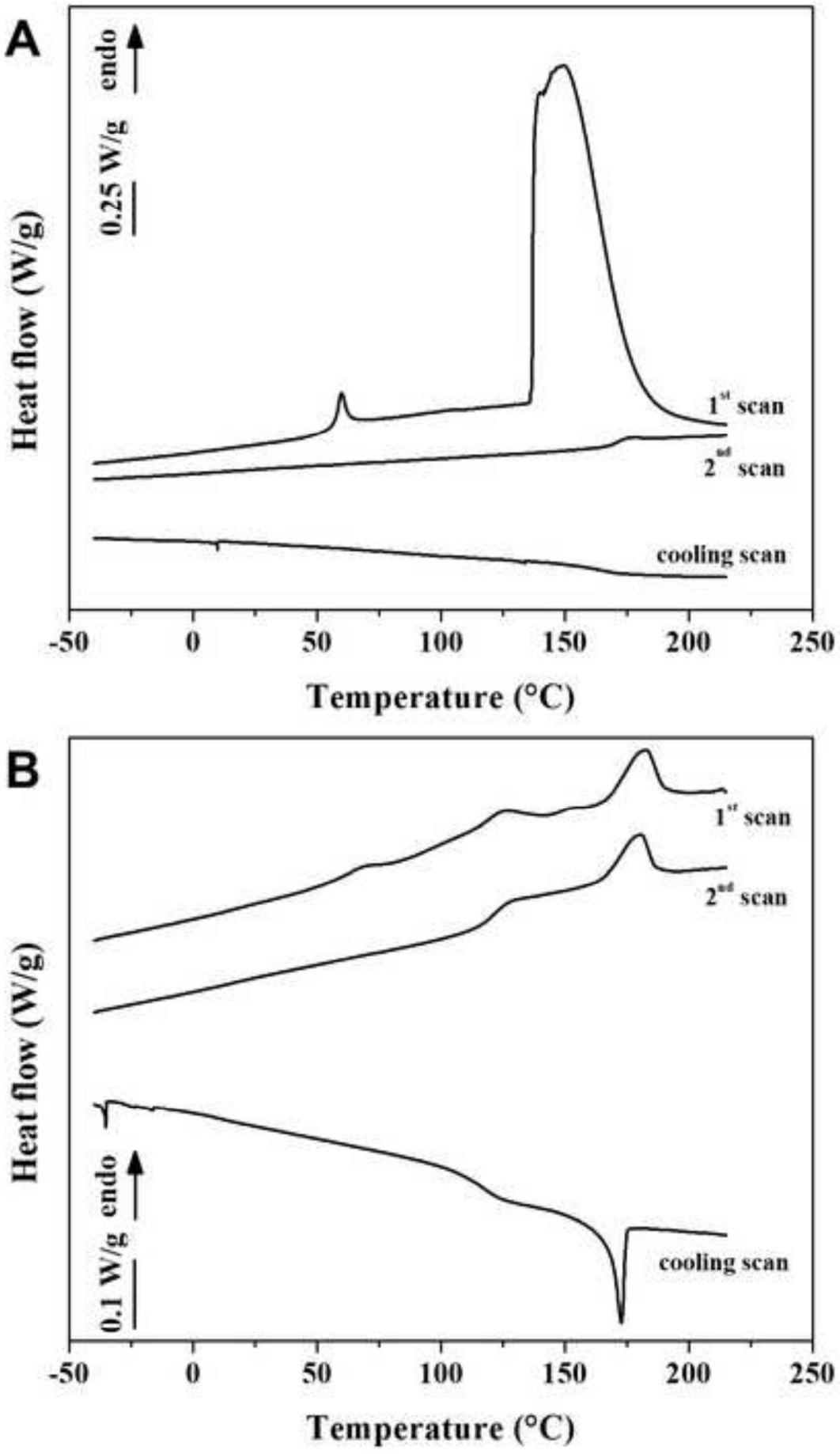

Figure

Click here to access/download;Figure;Figure 3.tif

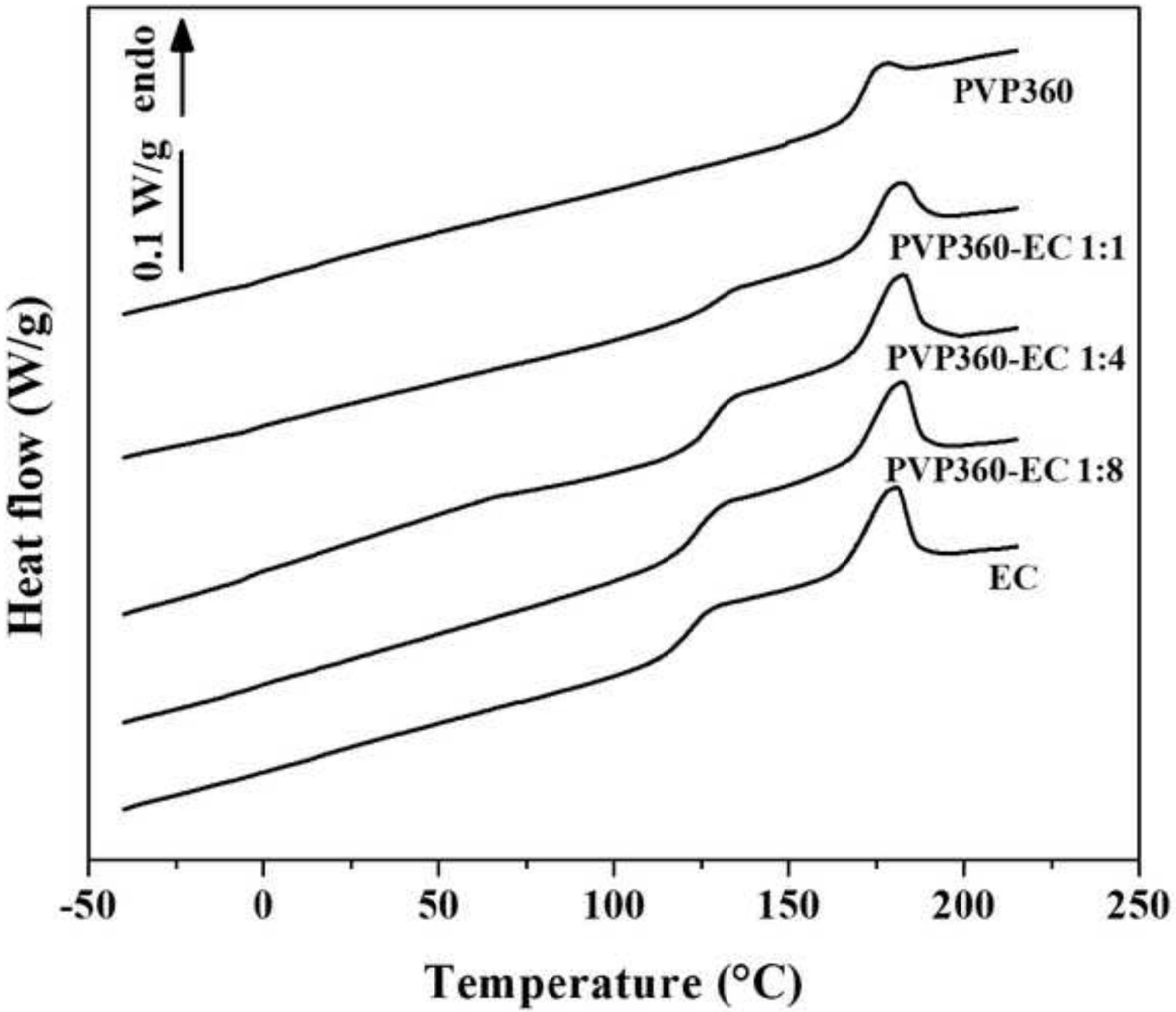

Figure

Click here to access/download;Figure;Figure 4.tif

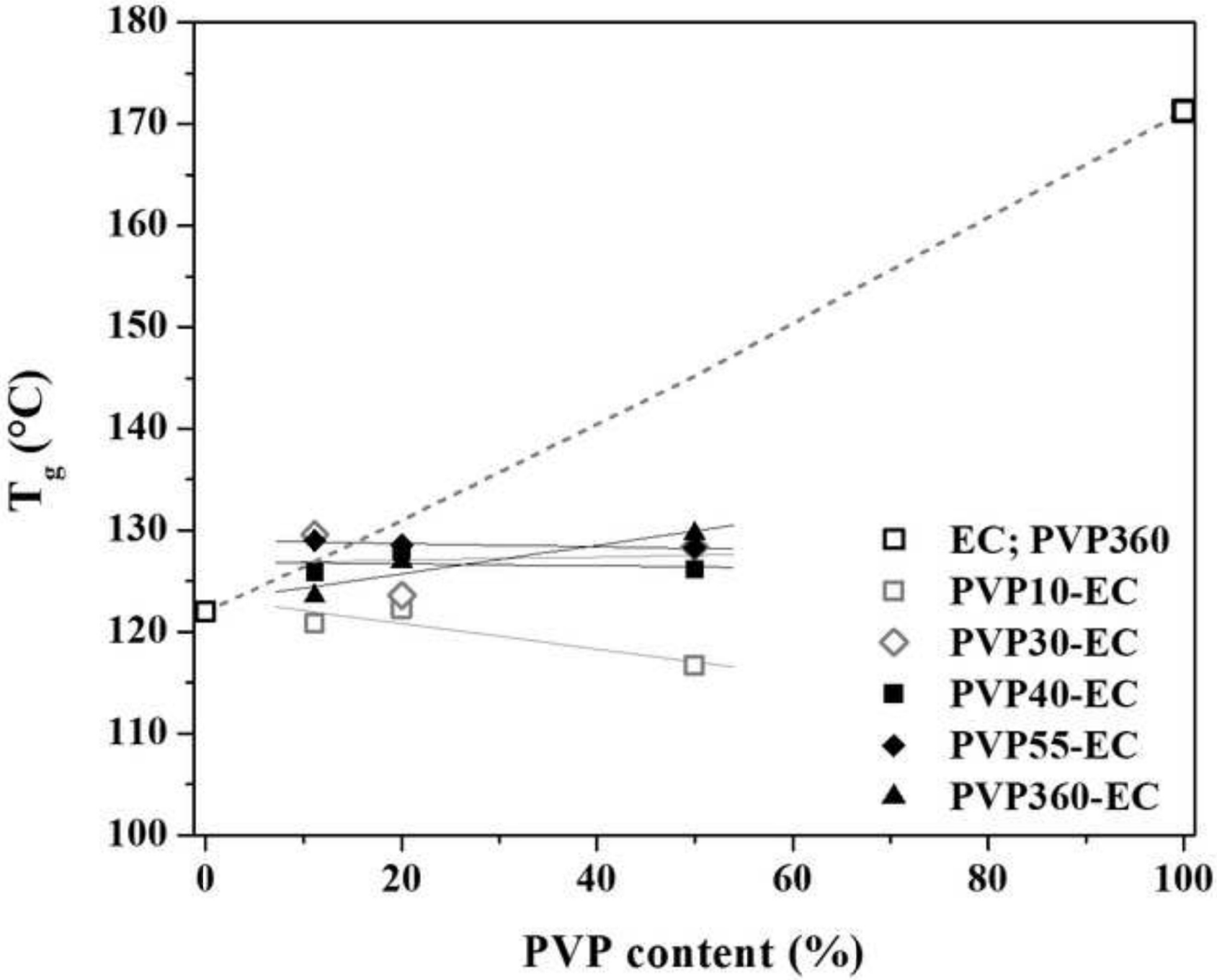

Figure

Click here to access/download;Figure;Figure 5.tif

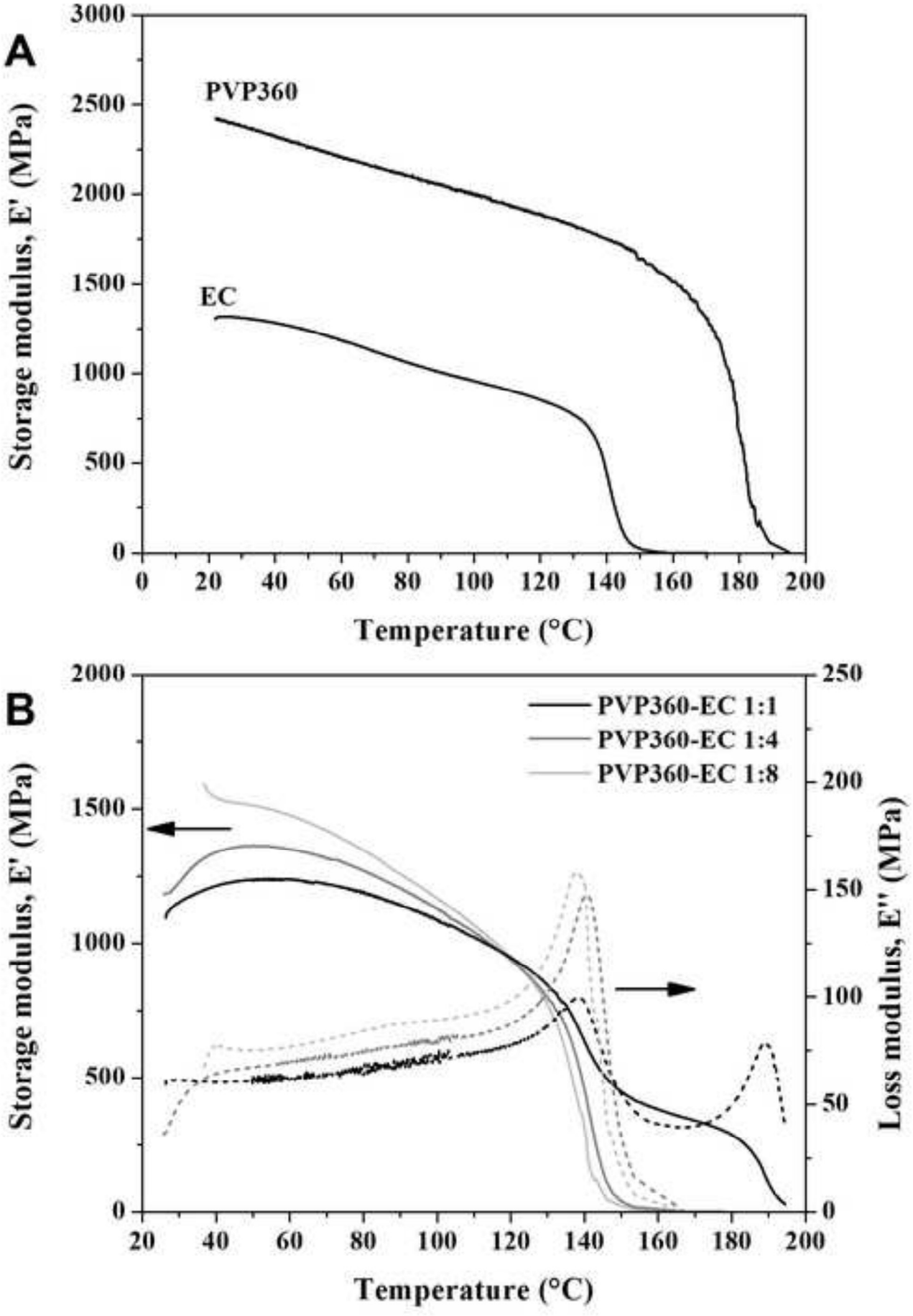

Figure

Click here to access/download;Figure;Figure 6.tif

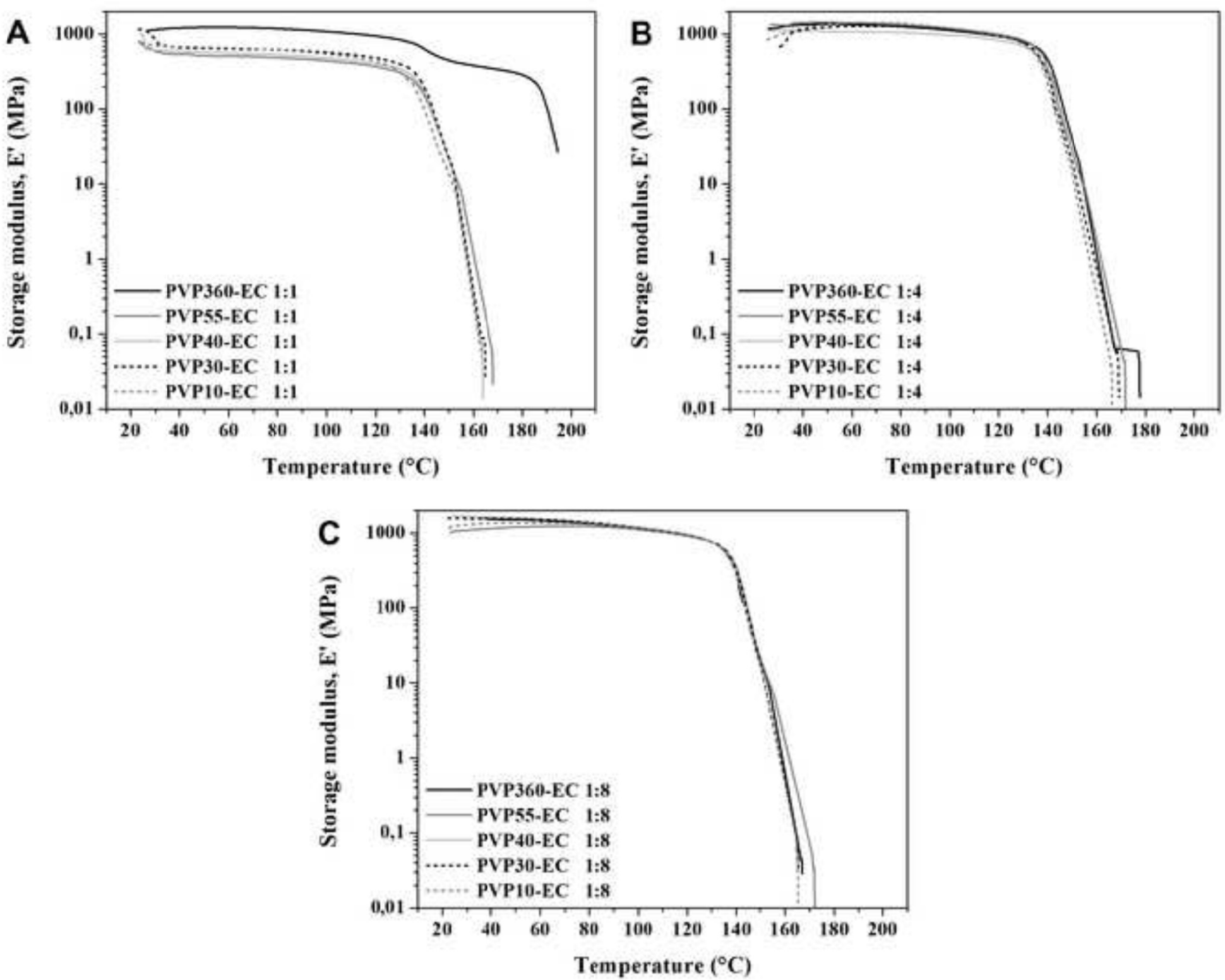

Figure

Click here to access/download;Figure;Figure 7.tif

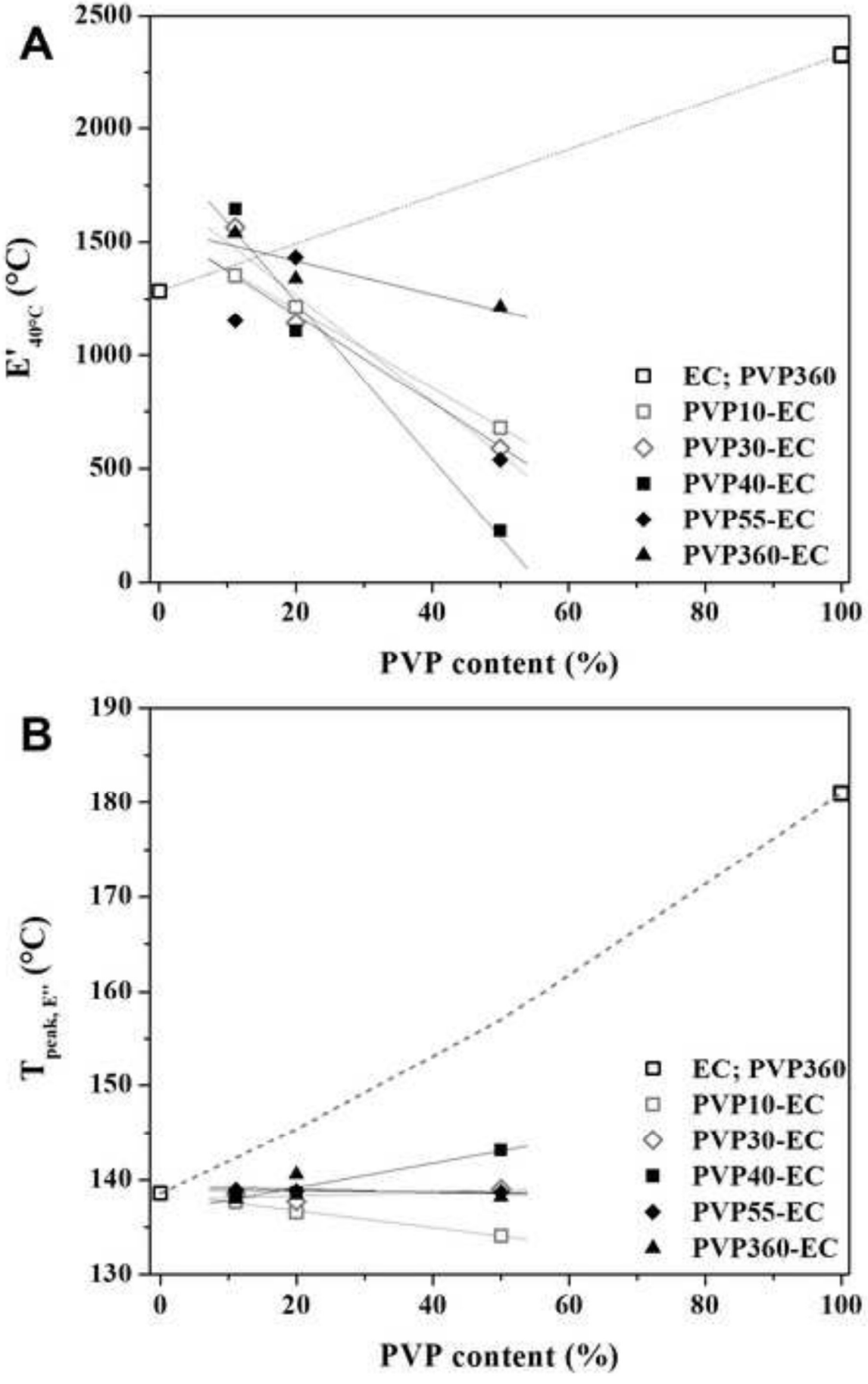

Figure

Click here to access/download;Figure;Figure 8.tif

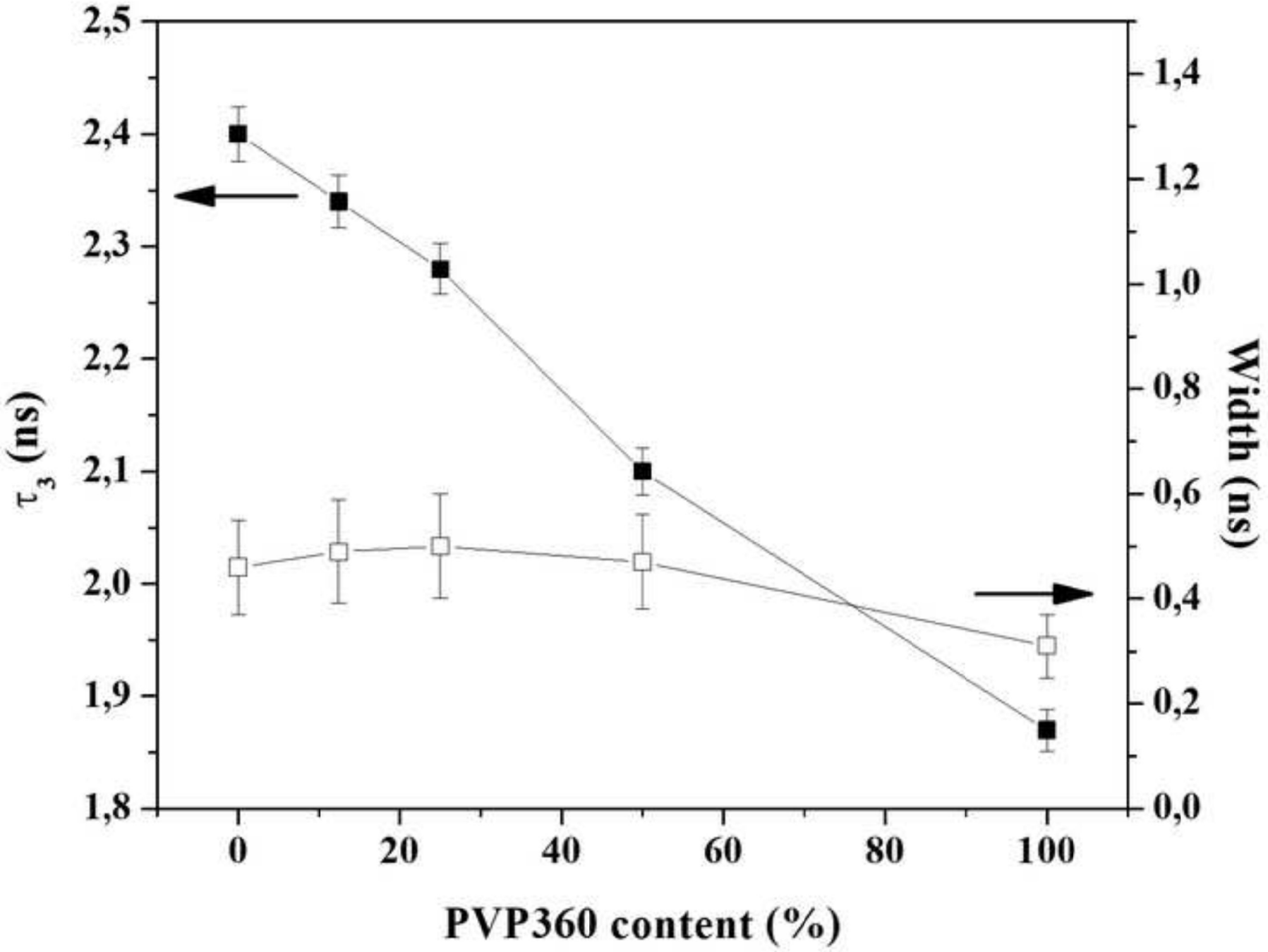

Figure

Click here to access/download;Figure;Figure 9 REVISED.tif

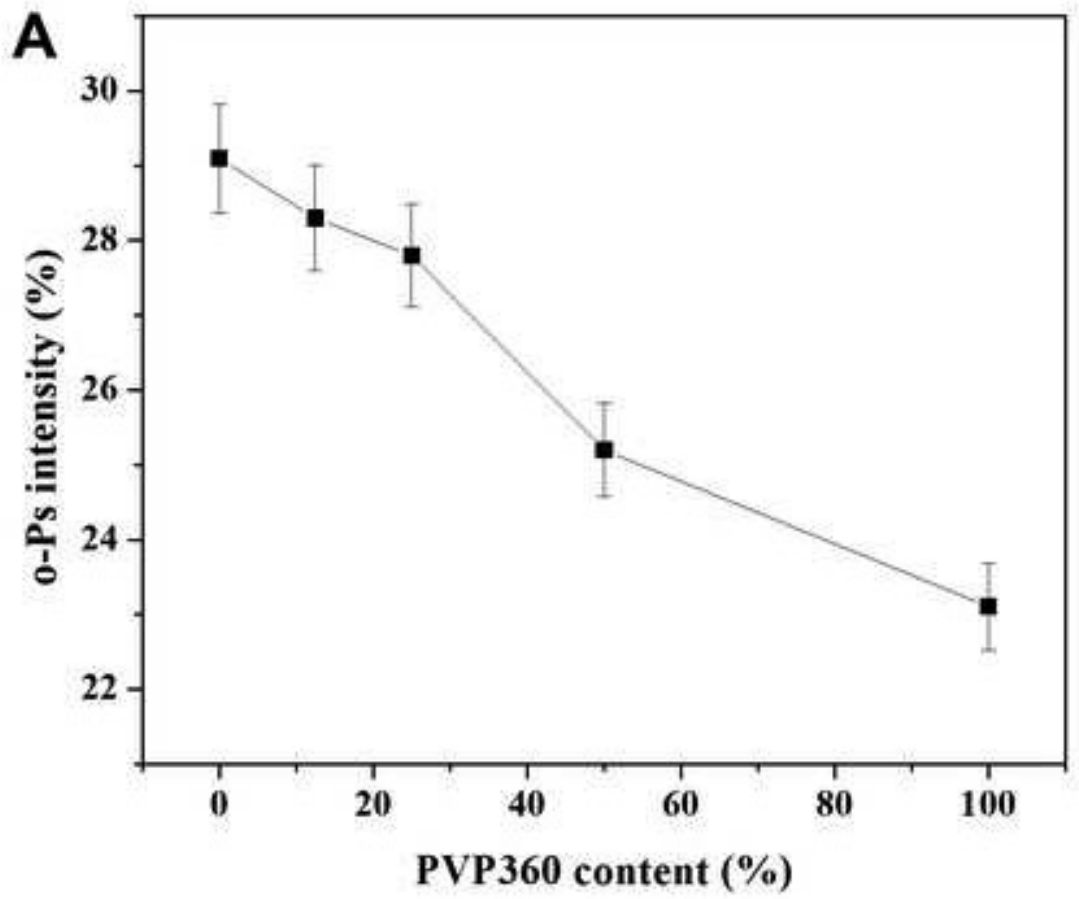

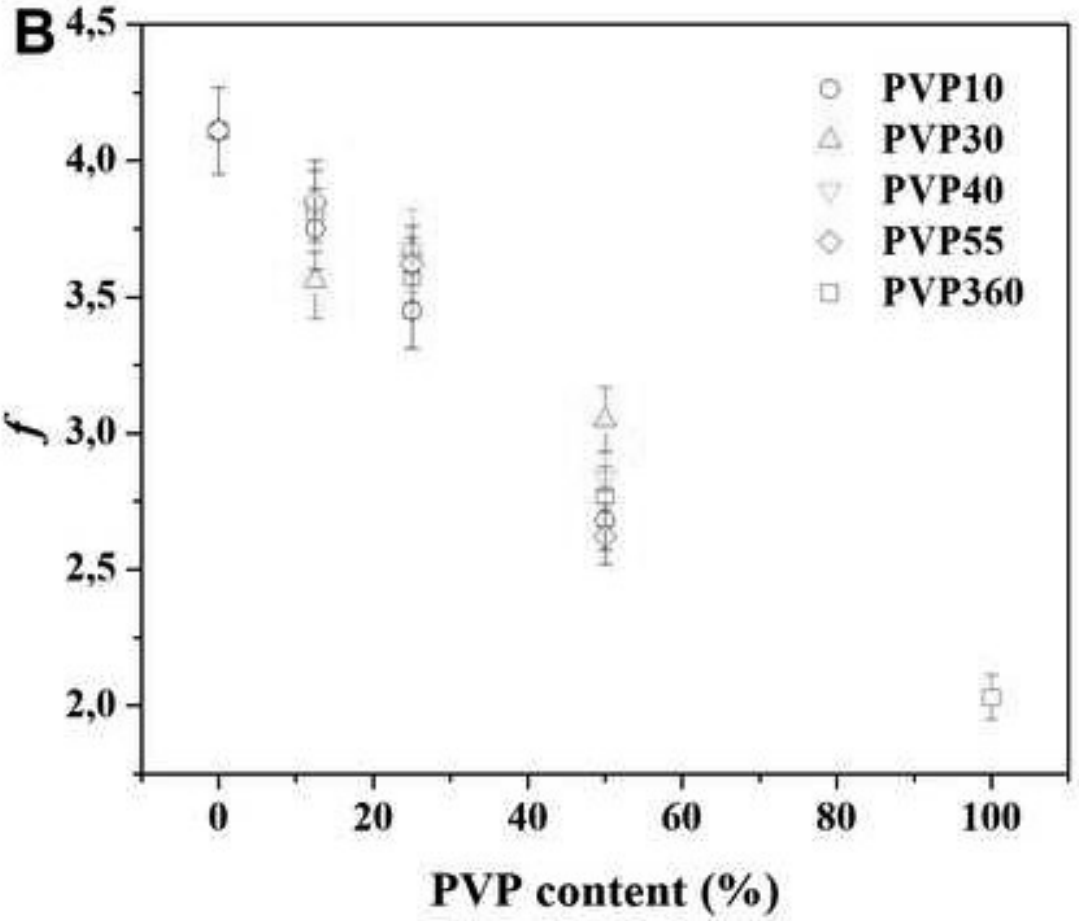

Figure

Click here to access/download;Figure;Graphical Abstract.jpg